AIP Journal of Applied Physics

Empirical determination of the energy band gap narrowing in p+ silicon heavily doped with boron

Di Yan and Andres Cuevas

Citation: Journal of Applied Physics **116**, 194505 (2014); doi: 10.1063/1.4902066
View online: http://dx.doi.org/10.1063/1.4902066
View Table of Contents: http://scitation.aip.org/content/aip/journal/jap/116/19?ver=pdfcov
Published by the AIP Publishing

Empirical determination of the energy band gap narrowing in p^+ silicon heavily doped with boron

Di Yan[a] and Andres Cuevas
Research School of Engineering, The Australian National University, Canberra ACT 0200, Australia

(Received 1 August 2014; accepted 7 November 2014; published online 19 November 2014)

In the analysis of highly doped silicon, energy band gap narrowing (BGN) and degeneracy effects may be accounted for separately, as a *net* BGN in conjunction with Fermi-Dirac statistics, or lumped together in an *apparent* BGN used with Boltzmann statistics. This paper presents an experimental study of silicon highly doped with boron, with the aim of evaluating the applicability of previously reported BGN models. Different boron diffusions covering a broad range of dopant densities were prepared, and their characteristic recombination current parameters J_0 were measured using a contactless photoconductance technique. The BGN was subsequently extracted by matching theoretical simulations of carrier transport and recombination in each of the boron diffused regions and the measured J_0 values. An evaluation of two different minority carrier mobility models indicates that their impact on the extraction of the BGN is relatively small. After considering possible uncertainties, it can be concluded that the BGN is slightly larger in p^+ silicon than in n^+ silicon, in qualitative agreement with theoretical predictions by Schenk. Nevertheless, in quantitative terms that theoretical model is found to slightly underestimate the BGN in p^+ silicon. With the two different parameterizations derived in this paper for the BGN in p^+ silicon, both statistical approaches, Boltzmann and Fermi-Dirac, provide a good agreement with the experimental data.
 [http://dx.doi.org/10.1063/1.4902066]

I. INTRODUCTION

The common use of highly doped regions in silicon devices, particularly in solar cells, has brought heavy-doping effects to the attention of many researchers over the years. In addition to a reduction of the minority carrier lifetime and mobility, the most important consequence of heavy doping is a change of the thermal equilibrium electron-hole product p_0n_0 compared to its low-doping value n_i.[2] The p_0n_0 product increases with dopant density due to energy band gap narrowing (BGN), and it decreases as a result of degeneracy effects and the subsequent need to use Fermi-Dirac statistics. A significant corpus of literature exists on experimental BGN data, for both highly doped n-type and p-type silicon.[1] For many years, during the extraction of BGN values from carrier transport measurements, different minority carrier mobility and lifetime assumptions were made by different authors, causing a relatively large disagreement amongst the published results. In 1992, Klaassen *et al.*,[2] continuing the line of work started by del Alamo *et al.*,[1] reexamined the data by applying a unified mobility model for minority carriers and an updated value of the intrinsic carrier concentration in silicon, n_i. The, thus, updated BGN values indicated a very small difference between n-type and p-type silicon, leading to the recommendation that a single BGN parameterization could be used for both. Nevertheless, such recommendation, and common practice among many researchers, is at odds with the theoretical work of Schenk,[3] which indicates that the BGN in n-type and p-type silicon should be expected to be different, slightly higher in p-type silicon.

To clarify the matter, we present here a detailed study of highly doped p-type silicon, complementing a similar recent study of highly doped n-type silicon.[4] The investigation is based on a broad range of boron diffused silicon samples, prepared in such a way to maximize the sensitivity to the BGN and minimize the impact of the minority carrier lifetime. The measured recombination current parameter of each diffused region J_0 is compared to computer simulations with Boltzmann statistics using the, until now, widely accepted *apparent* BGN model[5] (the same as for n-type silicon). Such exercise leads to a strong discrepancy between the measured and modelled J_0. The discrepancy does not disappear even if the modelling is done with Schenk's p-type BGN model[3] and Fermi-Dirac statistics. Therefore, an updated BGN model for p-type silicon is required.

In Secs. II–V, we present details of sample preparation and experimental characterization. The impact of the minority carrier parameters, mobility and Auger recombination, on the extraction of the BGN from the experimental measurements is then quantified. Finally, simple empirical models are derived to calculate either the *apparent* BGN (i.e., encompassing the effects of degeneracy) or the *net* BGN as a function of the dopant density.

II. EXPERIMENTAL METHODS

A diversity of dopant density profiles were produced by thermal boron diffusion, followed by oxidation/drive-in steps, on 100 Ω-cm high-resistivity n-type silicon wafers ($N_D = 4.43 \times 10^{13}\,cm^{-3}$) with a thickness of $400 \pm 20\,\mu m$. The boron pre-deposition step was performed within a temperature range of 900–1000 °C using BBr_3 as a dopant

[a]Electronic mail: di.yan@anu.edu.au

source. The drive-in step was carried out in pure oxygen at a temperature of 1000 °C for 10–100 min, after having removed the boron-silica glass. As a result, a total of 35 different dopant profiles, with sheet resistances between $19.6 \pm 0.2\,\Omega$/sq and $206.6 \pm 22\,\Omega$/sq and surface dopant concentrations from $(6.14 \pm 0.01) \times 10^{18}\,cm^{-3}$ to $(1.31 \pm 0.02) \times 10^{20}\,cm^{-3}$, were generated. The corresponding dopant density profiles, some of which are shown in Fig. 1, were measured using an electrochemical capacitance-voltage instrument (WEP Wafer Profile CVP21). This method gives the total concentration of substitutional, electrically active dopant atoms, which become ionized during the measurement. Incomplete ionization at room temperature,[6] whereas possible, is very small for the high dopant densities explored here; nevertheless, we have included incomplete ionization in the theoretical modelling. The surface dopant concentration was determined by matching the sheet resistance calculated from an integration of the dopant profile to the value measured with both a four point probe (Signatone, model S-301-4) and a calibrated inductive-coil conductance tester (Sinton Instruments, WCT 120).

After the thermal steps, all silicon oxides were removed from the surface in dilute HF and the wafers were cleaned in standard solutions based on ammonium hydroxide, hydrochloric acid, and hydrogen peroxide (RCA clean), plus another HF dip. Semi-transparent aluminum layers with a thickness of 10–20 nm were deposited on both sides of the wafers. For each metal-coated sample, that is, for every dopant profile, the recombination current density parameter J_0 was measured at room temperature by both transient photoconductance decay (PCD) and Quasi-Steady-State photoconductance (QSSPC), following the method described in Ref. 7, that is, by a linear fit of the inverse effective lifetime, corrected by Auger recombination in the highly injected silicon wafer,[8] at an excess carrier density in the range of $\Delta n = 0.5\text{–}1 \times 10^{15}\,cm^{-3}$. This simple method assumes that Δn is approximately constant over the wafer thickness. We re-analyzed the measurements using the numerical analysis procedure suggested in Ref. 9, which takes into account possible non-uniformities in excess carrier distribution. Even in the most extreme cases (highest J_0), we found that the maximum relative difference compared to the simple analysis is less than 10%, that is, smaller than the estimated overall experimental error of ±10%. The J_0 values at 300 K are plotted as a function of the sheet resistance of the diffusion in Fig. 2.

III. PREDICTION OF THE RECOMBINATION PARAMETER J_0 BY COMPUTER SIMULATION

It is straightforward to calculate the recombination current parameter J_0, which corresponds to a given dopant profile. A simple and flexible analytical minority-carrier transport model[10] has been used in this work, after confirming that it provides good accuracy in comparison to numerical simulations.[11] The physical material parameters required for the simulations are the minority carrier lifetime τ_n, the minority carrier mobility μ_n, the surface recombination velocity S_n, and the equilibrium p_0n_0 product. Since the surface is metalized, we have assumed that carriers reaching it do so at their thermal velocity, that is, the surface recombination velocity for electrons is $S_n = 3 \times 10^6\,cm/s$,[5] considering the one-dimensional restriction imposed by the surface plane on the random thermal motion of carriers (approximately a factor 1/3). We made the reasonable assumption that Auger recombination is dominant in heavily doped silicon, and that Shockley-Read Hall recombination is negligible. Therefore, we have computed τ_n as a function of dopant density using the empirical model proposed by Richter *et al.*[8] The minority electron mobility μ_n has been calculated with Klaassen's unified mobility model.[12] The uncertainty related to these assumptions is discussed below.

At high dopant concentrations, the thermal equilibrium p_0n_0 product changes with respect to its normal value n_i^2 (the intrinsic carrier density in lowly doped silicon is

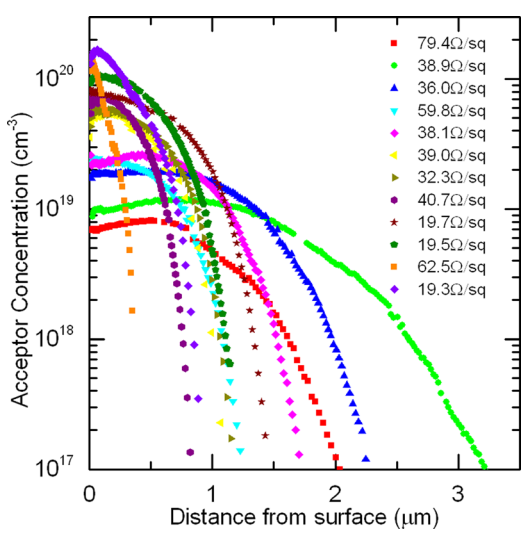

FIG. 1. Electrically active boron concentration profiles of several silicon samples with different sheet resistances and acceptor concentrations.

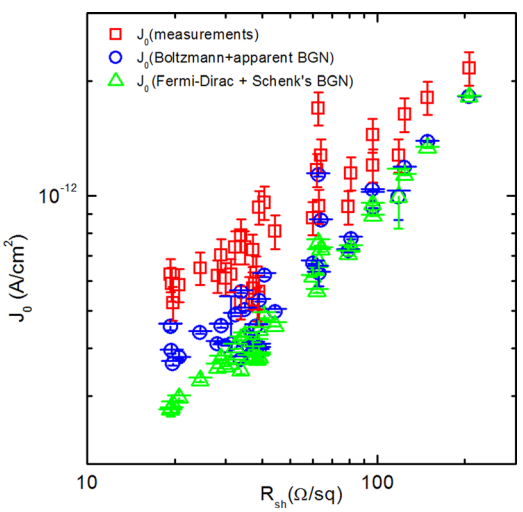

FIG. 2. Measured recombination current parameter J_0 as a function of the sheet resistance of the boron diffusions, compared to computer simulations based on Fermi-Dirac statistics with Schenk's BGN, or Boltzmann statistics with the same apparent BGN as that of n-type silicon.

$n_i = 9.65 \times 10^9\,cm^{-3}$ at 300 K (Ref. 13)) due to energy bandgap narrowing ΔE_g and to Fermi-Dirac statistics. An *effective* intrinsic carrier concentration n_{ieff} can be determined as

$$p_0 \cdot n_0 = n_{ieff}^2 = n_i^2 \frac{\frac{n_o}{N_c}}{\exp\left(F_{1/2}^{-1}\left(\frac{n_o}{Nc}\right)\right)} \exp\left(\frac{\Delta E_g}{KT}\right). \quad (1)$$

Alternatively, the use of Boltzmann statistics may be forced, leading to an *apparent* BGN ΔE_g^{app} defined as

$$p_0 \cdot n_0 = n_{ieff}^2 = n_i^2 \exp\left(\frac{\Delta E_g^{app}}{KT}\right). \quad (2)$$

We have performed the simulations in two different scenarios. The first following Eq. (1), with Schenk's theoretical BGN model[3] for p-type silicon together with Fermi-Dirac statistics. The second, quite extended in the research community, using an *apparent* BGN parameterization identical to that reported for n-type silicon,[5] together with Boltzmann statistics, as per Eq. (2). The resulting values of the p_0n_0 product are plotted in Fig. 3 as a function of the dopant concentration in p-type silicon, assumed to be equal to the majority carrier (hole) concentration. It can be observed that BGN effects tend to increase the p_0n_0 product, hence the minority carrier concentration. But once the dopant concentration surpasses the effective density of states in the valence band N_v, which has a value close to $3 \times 10^{19}\,cm^{-3}$, degeneracy effects start reducing the p_0n_0 product. In other words, degeneracy effects partially compensate for the consequences of BGN. Fig. 3 shows that the two calculations of the p_0n_0 product are almost identical over a broad range of dopant densities, but they diverge at very high dopant concentrations. This indicates that the parameterization used here for ΔE_g^{app} does not perfectly account for degeneracy effects for dopant densities in the vicinity of $1 \times 10^{20}\,cm^{-3}$ and above.

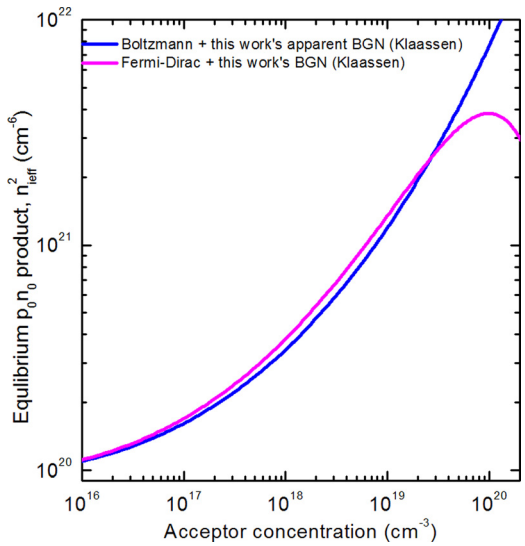

FIG. 3. Equilibrium p_0n_0 product in highly doped p^+ silicon, computed with either Boltzmann or Fermi-Dirac statistics with the corresponding empirical expressions for the energy band gap narrowing derived in this paper and Klaassen's minority carrier mobility.

A comparison between the simulated and experimental J_0 values for all the samples fabricated for this study is presented in Fig. 2. As can be observed, the n-type *apparent* BGN model[5] and Boltzmann statistics cannot reproduce the measurements of J_0 accurately. The second scenario based on Schenk's BGN model and Fermi-Dirac statistics leads to an even stronger disagreement with the experimental J_0 values. The discrepancies are greater for the diffusions with the lowest sheet resistances, that is, with the highest dopant concentrations. Since both simulation scenarios underestimate the recombination current density J_0, the experiments indicate that the BGN in highly doped p^+ silicon is likely higher than previously thought.

IV. EXTRACTION OF THE ENERGY BANDGAP NARROWING IN P^+ SILICON

The difference between experimental and simulated J_0 values indicates that a reevaluation of the BGN in heavily doped p-type silicon is necessary. The objective of this section is to derive an empirical BGN model as a function of dopant density that provides consistency between the simulated and the measured J_0 values. As a starting point, we assume a simple expression for the BGN as a function of dopant concentration

$$\Delta E_g(N_A) = A\left[\ln\left(\frac{N_A}{N_{ref}}\right)\right]^b + C, \quad (3)$$

where A, b, and C are constants and N_{ref} represents a reference dopant concentration where BGN effects are still negligible. This expression provides a good fit to Schenk's theoretical BGN model when $C = 0$, $b = 3$, $N_{ref} = 1 \times 10^{14}\,cm^{-3}$, and $A = 4.20 \times 10^{-5}\,eV$. Based on that we fix three of the constants in Eq. (3) to $C = 0$, $b = 3$, and $N_{ref} = 1 \times 10^{14}\,cm^{-3}$, and then we iteratively perform simulations for each dopant profile until a value of the constant A is found by matching the simulated J_0 and the measured J_0. The results of such procedure for the 35 different boron diffusions are given in Table III of the Appendix. Despite the diversity of dopant profiles in the study, they all lead to quite similar values of the constant A; averaging all of them we determine a global value of the parameter A which approximately represents BGN effects in all of them collectively. By repeating the analysis twice, once with Boltzmann statistics and a second time using Fermi-Dirac statistics, we obtain two different values of the constant A, the first corresponding to the *apparent* BGN ($A = 4.32 \times 10^{-5}\,eV$), and the second to the *net* BGN ($A = 4.72 \times 10^{-5}\,eV$). Alternatively, some of the most commonly used apparent BGN models[5,14,15] are based on a simpler expression with $b = 1$ and $C = 0$; in this case, a value of $N_{ref} = 1 \times 10^{17}\,cm^{-3}$ gives the best fit to our experimental data, with a resulting constant $A = 1543 \times 10^{-5}\,eV$. The values of the constants associated with each of the different BGN models are summarized in Table II. These calculations are based on an intrinsic carrier concentration of $n_i = 9.65 \times 10^9\,cm^{-3}$ at a temperature of 300 K.

TABLE I. Measured recombination current density J_0 of two boron profiles with similar surface concentrations but different sheet resistances. The surface was metalized with aluminium.

	N_{surf} (cm^{-3})	R_{sh} (Ω/sq)	J_0 (A/cm^3)
Sample 1	3.39×10^{19}	35	7.36×10^{-13}
Sample 2	3.44×10^{19}	62	1.17×10^{-12}

We have evaluated the possible influence of incomplete ionization and confirmed that the difference in the constant A that results from including or not an incomplete ionization model[16,17] is within the error range of the results, as given in Table II. Therefore, the impact of incomplete ionization is negligible in this work.

A. Uncertainties in BGN extraction due to carrier mobility and lifetime

In addition to measurement error, indicated by the error bars in Fig. 2, the extraction of the BGN via modeling may be affected by the remaining carrier transport and recombination parameters. In particular, the minority carrier lifetime may be affected by the presence of defects or dopant precipitates, or simply by the uncertainties in the Auger recombination parameters. To minimize its impact, we have designed the experiment so that the total recombination in the diffused region happens mostly at the surface, rather than in the volume. We ensured a very high surface recombination velocity by directly depositing aluminum onto the silicon. This means that carrier recombination is limited by the supply of carriers towards the surface, that is, by the minority diffusivity (or mobility). An approximate, first order solution for such transport-limited recombination regime is[10]

$$J_{op^+} = \left(\int_0^{W_{p^+}} \frac{1}{q n_0 D_n} dx \right)^{-1}, \quad (4)$$

where q is the elementary charge, W_{p+} is the width of the diffused region, n_0 is the equilibrium electron density (within which the BGN is embedded), and D_n is the minority carrier diffusion coefficient. As Eq. (4) indicates a high carrier mobility or a short distance to be covered by the carriers in their trip to the surface will result in a large recombination parameter J_0, and vice versa. This can be illustrated by comparing two dopant profiles with similar surface dopant concentration and different diffusion depth, as those in Table I. Transport to the surface occurs more readily for the thinner diffusion, especially when it is shorter than the diffusion length of minority carriers, leading to a higher J_0.

Generally, Auger recombination in the subsurface region represents only a small amount of the total recombination in the transport limited case, and this drastically reduces the impact of Auger recombination model in the simulation of these samples. To confirm this, we applied different Auger recombination models by Dziewior and Schmid,[18] Kerr and Cuevas,[19] Altermatt *et al.*,[20] and Richter *et al.*,[8] to the analysis, and found that the resulting J_0 values are very similar, changing by less than 1% for all the samples.

TABLE II. Characteristic parameter A corresponding to the two empirical BGN models, *net* ΔE_g and *apparent* ΔE_g^{app}, derived in this paper using the minority carrier mobility of either Klaassen *et al.* or Swirhun *et al.* The BGN parameters for n^+ silicon derived in Ref. 4 are included for comparison. For the calculation with the third order function Eq. (1), values of $C = 0$ and $N_{ref} = 1 \times 10^{14}\,cm^{-3}$ were used. For the apparent BGN model with $b = 1$, last two rows in the table, constant values of $C = 0$ and $N_{ref} = 1 \times 10^{17}\,cm^{-3}$ were used.

	Dopant type	Statistics	Mobility model	A ($\times 10^{-5}$ eV)	b
ΔE_g^{app}	N^+	Boltzmann	Klaassen	(3.67 ± 0.20)	3
ΔE_g	N^+	Fermi-Dirac	Klaassen	(4.20 ± 0.30)	3
ΔE_g^{app}	p^+	Boltzmann	Klaassen	(4.32 ± 0.12)	3
ΔE_g^{app}	p^+	Boltzmann	Swirhun	(4.12 ± 0.15)	3
ΔE_g	p^+	Fermi-Dirac	Klaassen	(4.72 ± 0.12)	3
ΔE_g	p^+	Fermi-Dirac	Swirhun	(4.53 ± 0.16)	3
ΔE_g^{app}	p^+	Boltzmann	Klaassen	(1543 ± 46)	1
ΔE_g	p^+	Boltzmann	Swirhun	(1476 ± 48)	1

On the other hand, Eq. (4) indicates that the extraction of the BGN (via n_0) is affected by the assumed carrier mobility. We have investigated the impact on the simulations of two different mobility parameterizations, proposed by Klaassen *et al.*[12] and by Swirhun *et al.*,[21] respectively. These two empirical mobility models, together with relevant experimental data, are illustrated in Fig. 4. Although the difference between both mobility models is less than the scatter in experimental data, Klaassen's model gives a slightly lower minority electron mobility in highly doped p-type silicon ($>2 \times 10^{17}\,cm^{-3}$). As shown by Eq. (4), lower mobility values result in lower recombination parameters J_0, hence, to achieve a given J_0 with a lower mobility a higher BGN will be needed. Therefore, Klaassen's mobility model can be

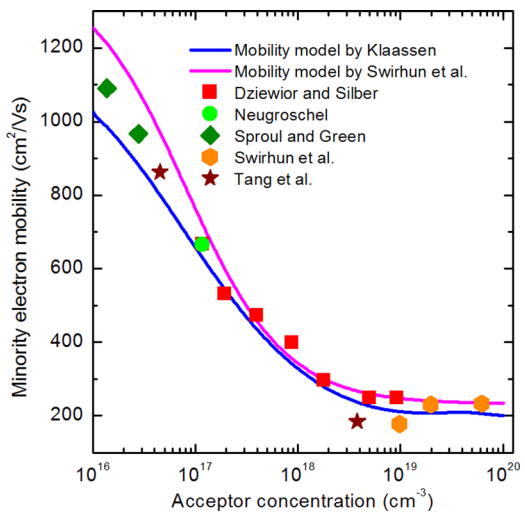

FIG. 4. Minority electron mobility as a function of dopant concentration calculated with Klaassen (blue line) and Swirhun *et al.* (pink line) parameterizations. Experimental measurements by Dziewior and Sliber,[22] Neugroschel,[23] Sproul *et al.*,[24] Swirhun *et al.*,[21] and Tang *et al.*[25] are represented as symbols.

expected to result in a slightly higher BGN than Swirhun's model in the analysis of our experiments.

We have repeated the analysis of all the 35 samples using either Klaassen's mobility model or the mobility model of Swirhun *et al.*, together with the Auger recombination model of Ref. 8, noting that the specific bulk recombination model plays only a minor role in the samples analyzed here. A surface recombination velocity of 3×10^6 cm/s is used as the boundary condition at the metal coated surface. The results of the analysis, that is, the values of the coefficient A corresponding to each of the two mobility models and to either the *apparent* BGN or *net* BGN are summarized in Table II. As expected, the coefficient A that results from using Klaassen's mobility model is larger than that from Swirhun's model, but the main point is that the difference between them is relatively small; in fact, the corresponding error margins overlap.

The BGN parameters for n-type silicon, determined in Ref. 4, are also shown in Table II. Irrespective of which mobility model is assumed, either Klaassen's or Swirhun's, the BGN extracted from the p-type boron diffused samples is larger than that for n-type phosphorus diffused regions, which is qualitatively consistent with theoretical studies.[3]

B. Comparison between BGN models

The four variants of the empirical BGN expression for boron doped silicon given in Table II are graphically compared in Fig. 5 to Schenk's theoretical BGN model (yellow continuous line) as well as to previously published experimental data for p+ silicon. The *net* and *apparent* BGN parameterizations derived from the mobility model of Swirhun *et al.* are shown as continuous lines (red for Fermi-Dirac and green for Boltzmann). The curve for the *apparent* $\Delta E_g{}^{app}$ extracted with Swirhun's mobility model falls on top of Schenk's *net* ΔE_g, which of course is merely coincidental, since the latter is based on Fermi-Dirac statistics and the former is not. The relevant comparison is between Schenk's model and the *net* ΔE_g derived in this paper (red continuous line); the experimental results from this study indicate that the *net* ΔE_g in boron doped silicon is higher than predicted by Schenk's theoretical model (by about 10 meV at 1×10^{20} cm^{-3}). It should be noted that the experiments in this paper support the BGN empirical models only up to a dopant density of 1.3×10^{20} cm^{-3}.

The discontinuous lines represent both the *net* and *apparent* BGN models obtained from Klaassen's mobility model (red for Fermi-Dirac and blue for Boltzmann). For a given statistical model, the BGN values extracted with Klaassen's mobility are always higher than those derived with Swirhun's mobility. The four BGN expressions are in reasonably good agreement with previously reported experimental data. In fact, the differences between the BGN expressions due to different statistics or to different mobility models are smaller than the scatter in those experimental data. Over the full range of dopant concentrations explored here, the *net* BGN ΔE_g is higher than the *apparent* BGN $\Delta E_g{}^{app}$, the discrepancy between them becoming more pronounced at the higher dopant concentrations. A good correlation can be observed between the *net* ΔE_g derived with the

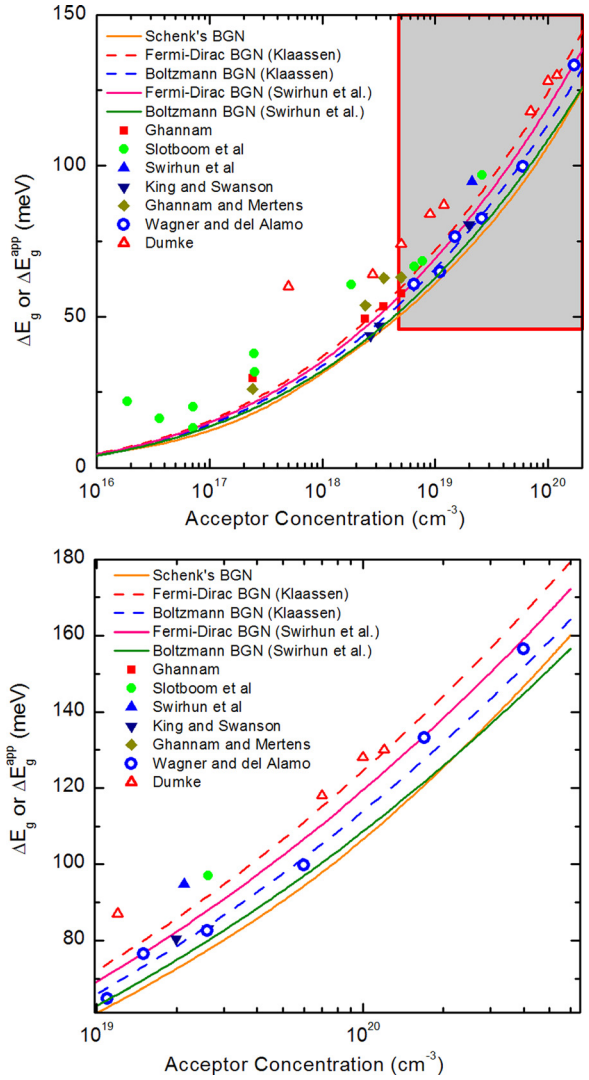

FIG. 5. Energy bandgap narrowing as a function of dopant concentration in heavily doped p-type silicon. The dashed lines represent BGN models derived by using mobility of Swrihun *et al.* The continuous lines represent BGN models obtained from Klaassen's mobility, as well as Schenk's theoretical p-type BGN model. Electronic measurements by Slotboom and de Graaff,[28] Swirhun *et al.*,[21] King and Swanson,[29] and Ghannam and Mertens.[27] They were re-calculated with Klaassen's mobility model and $n_i = 9.65 \times 10^9$ cm^{-3}. Photoluminescence measurements from Wagner and del Alamo[26] and Dumke.[30] The bottom shows the enlarged figure of the shadow region of top figure. It is in a dopant range from 10^{19} cm^{-3} to 6×10^{20} cm^{-3}.

mobility model of Swirhun *et al.* and the photoluminescence measurements of the BGN by Wagner and del Alamo;[26] such agreement is significant, since photoluminescence measurements also give the *net* ΔE_g. Based on this agreement, it appears that the mobility expression proposed by Swirhun *et al.* is more appropriate for highly doped p-type silicon than the more widely used model of Klaassen, although the difference between the resulting expressions for the BGN is relatively small.

V. CONCLUSION

In this paper, updated BGN models for boron doped p^+ silicon have been derived from a combination of experimental measurements and computer simulations. The well-established approach to model minority carrier transport and

recombination in highly doped p-type silicon, based on Fermi-Dirac statistics and Schenk's theoretical BGN, underestimates the recombination parameter J_0 for all the boron diffusions prepared for this study; the level of underestimation being up to a factor of 2.3 for the most heavily doped diffusions. A second approach, also quite extended among the scientific community, has been based on assuming that the *apparent* BGN in p^+ silicon is approximately the same as in n^+ silicon, together with Boltzmann statistics. Again, we have found that such approach underestimates J_0, up to a factor of 1.8 in some samples. Our measurements strongly indicate that the BGN in p^+ silicon is higher than in n^+ silicon.

To achieve a good agreement between modelled and measured recombination parameter J_0, it is necessary to use the empirical expression for the BGN derived in this paper. Two of them, one for the *apparent* BGN and another for the *net* BGN, have been derived. They are approximately equivalent to each other, as long as they are used with the appropriate carrier statistics, either Boltzmann or Fermi-Dirac. These expressions are the result of an averaging procedure over 35 different boron diffused samples, which are representative of most boron diffused regions used in silicon solar cell technology. Nevertheless, the highest dopant density explored in this paper is $1.3 \times 10^{20}\,cm^{-3}$, and in each of those samples the dopant concentration varies with position, which means that the ΔE_g extracted from each of them is the result of a weighted average of BGN effects over the full thickness of the diffused region. Despite those limitations, the proposed empirical expressions are appropriate to model the recombination current of a broad range of boron doped regions.

APPENDIX: SUMMARY OF THE BORON DIFFUSED SAMPLES

TABLE III. Summary of the boron diffusions used in this work, including sheet resistance and surface concentration. The J_0 measurements of the aluminium coated diffusions are shown, and revaluated for $n_i = 9.65 \times 10^9\,cm^{-3}$. The corresponding coefficients A calculated by using either Boltzmann or Fermi-Dirac statistics in different mobility models (Klaassen and Swirhun) are also shown. Constants, $b = 3$, $N_{ref} = 10^{14}\,cm^{-3}$, and $C = 0$, are used for these calculations.

Sample	Ns (cm^{-3})	Diffusion depth (μm)	R_{sh} (Ω/sq)	J_0 (measured) (A/cm^2)	A (Fermi-Dirac + Klaassen) ($\times 10^{-5}$ eV)	A (Boltzmann + Klaassen) ($\times 10^{-5}$ eV)	A (Fermi-Dirac + Swirhun) ($\times 10^{-5}$ eV)	A (Boltzmann + Swirhun) ($\times 10^{-5}$ eV)
1	6.14×10^{18}	1.02	206.65	2.16×10^{-12}	4.38	4.27	4.13	4.02
2	6.91×10^{18}	2.10	79.41	9.38×10^{-13}	4.58	4.44	4.32	4.18
3	8.71×10^{18}	3.74	38.98	5.12×10^{-13}	4.61	4.43	4.35	4.18
4	9.32×10^{18}	3.27	38.55	5.23×10^{-13}	4.65	4.48	4.39	4.23
5	1.04×10^{19}	0.95	148.74	1.81×10^{-12}	4.56	4.40	4.31	4.15
6	1.11×10^{19}	1.24	96.34	1.20×10^{-12}	4.53	4.34	4.28	4.09
7	1.24×10^{19}	1.05	124.10	1.63×10^{-12}	4.65	4.47	4.41	4.22
8	1.36×10^{19}	2.53	39.04	5.62×10^{-13}	4.67	4.45	4.43	4.21
9	1.50×10^{19}	1.41	81.11	1.15×10^{-12}	4.77	4.57	4.53	4.33
10	1.67×10^{19}	1.41	62.88	9.42×10^{-13}	4.64	4.39	4.42	4.17
11	1.69×10^{19}	2.52	37.11	5.74×10^{-13}	4.66	4.41	4.44	4.19
12	1.71×10^{19}	2.53	36.02	5.59×10^{-13}	4.66	4.40	4.44	4.18
13	1.82×10^{19}	2.95	33.74	5.29×10^{-13}	4.70	4.45	4.48	4.23
14	2.13×10^{19}	0.77	96.10	1.44×10^{-12}	4.62	4.32	4.42	4.11
15	2.27×10^{19}	1.27	59.78	8.79×10^{-13}	4.55	4.25	4.34	4.05
16	2.32×10^{19}	1.59	44.31	8.09×10^{-13}	4.87	4.59	4.66	4.38
17	2.46×10^{19}	1.78	37.13	7.23×10^{-13}	4.90	4.60	4.70	4.39
18	2.61×10^{19}	1.80	38.13	6.32×10^{-13}	4.63	4.31	4.43	4.11
19	3.01×10^{19}	1.79	29.91	6.09×10^{-13}	4.73	4.33	4.56	4.16
20	3.39×10^{19}	1.23	34.87	7.36×10^{-13}	4.69	4.23	4.53	4.07
21	3.44×10^{19}	1.01	61.99	1.17×10^{-12}	4.97	4.52	4.80	4.36
22	3.55×10^{19}	1.07	39.01	9.37×10^{-13}	4.94	4.44	4.79	4.28
23	3.56×10^{19}	1.73	31.29	6.23×10^{-13}	4.75	4.36	4.57	4.18
24	3.70×10^{19}	1.58	28.05	6.19×10^{-13}	4.74	4.29	4.58	4.13
25	4.30×10^{19}	1.24	32.31	7.37×10^{-13}	4.75	4.22	4.60	4.06
26	4.82×10^{19}	1.22	28.85	7.03×10^{-13}	4.77	4.23	4.63	4.08
27	5.16×10^{19}	0.62	63.83	1.28×10^{-12}	4.71	4.21	4.56	4.05
28	5.45×10^{19}	0.82	40.67	9.63×10^{-13}	4.81	4.18	4.66	4.03
29	6.86×10^{19}	1.44	20.69	5.85×10^{-13}	4.81	4.17	4.66	4.02
30	8.33×10^{19}	1.49	19.68	5.25×10^{-13}	4.72	4.08	4.58	3.94
31	8.94×10^{19}	1.25	24.43	6.49×10^{-13}	4.81	4.12	4.66	3.97
32	9.27×10^{19}	1.14	19.50	5.89×10^{-13}	4.83	4.04	4.69	3.89
33	9.87×10^{19}	0.95	33.86	7.92×10^{-13}	4.75	4.07	4.60	3.91
34	1.14×10^{19}	0.35	62.50	1.66×10^{-12}	4.88	4.01	4.73	3.86
35	1.31×10^{19}	0.96	19.32	6.23×10^{-13}	4.86	3.86	4.72[2]	3.71

[1]J. del Alamo, S. Swirhun, and R. M. Swanson, Solid-State Electron. **28**, 47–54 (1985).
[2]D. B. M. Klaassen, J. W. Slotboom, and H. C. de Graaff, Solid-State Electron. **35**, 125–129 (1992).
[3]A. Schenk, J. Appl. Phys. **84**, 3684–3695 (1998).
[4]D. Yan and A. Cuevas, J. Appl. Phys. **114**, 044508 (2013).
[5]A. Cuevas, P. A. Basore, G. Giroult-Matlakowski, and C. Dubois, J. Appl. Phys. **80**, 3370–3375 (1996).
[6]M. Rauer, M. Rüdiger, C. Schmiga, H. Strutzberg, M. Bähr, M. Glatthaar, and S. W. Glunz, J. Appl. Phys. **114**, 203702 (2013).
[7]D. E. Kane and R. M. Swanson, in *IEEE Photovoltaic Specialists Conference* (IEEE, 1985), pp. 578–583.
[8]A. Richter, S. W. Glunz, F. Werner, J. Schmidt, and A. Cuevas, Phys. Rev. B **86**, 165202 (2012).
[9]T. Andrew, G. Nicholas, C. Kean Fong, and K. Teng, Proceedings of the 4th International Conference on Crystalline Silicon Photovoltaics, Vol. 55 (Energy Procedia, 2014), pp. 141–148.
[10]A. Cuevas, R. Merchan, and J. C. Ramos, IEEE Trans. Electron Devices **40**, 1181–1183 (1993).
[11]K. R. McIntosh and P. P. Altermatt, in *35th IEEE Photovoltaic Specialists Conference (PVSC)* (IEEE, 2010), pp. 2188–2193.
[12]D. B. M. Klaassen, Solid-State Electron. **35**, 953–959 (1992).
[13]K. Misiakos and D. Tsamakis, J. Appl. Phys. **74**, 3293–3297 (1993).
[14]J. del Alamo, S. Swirhun, and R. M. Swanson, Int. Electron Devices Meet. **31**, 290–293 (1985).
[15]P. A. Basore, IEEE Trans. Electron Devices **37**, 337–343 (1990).
[16]A. Schenk, P. P. Altermatt, and B. Schmithusen, in *2006 International Conference on Simulation of Semiconductor Processes and Devices* (IEEE, 2006), pp. 51–54.
[17]P. P. Altermatt, A. Schenk, B. Schmithusen, and G. Heiser, J. Appl. Phys. **100**, 113715 (2006).
[18]J. Dziewior and J. Schmid, Appl. Phys. Lett. **31**, 346–348 (1977).
[19]M. J. Kerr and A. Cuevas, J. Appl. Phys. **91**, 2473–2480 (2002).
[20]P. P. Altermatt, J. Schmidt, G. Heiser, and A. G. Aberle, J. Appl. Phys. **82**, 4938–4944 (1997).
[21]S. E. Swirhun, Y. H. Kwark, and R. M. Swanson, Int. Electron Devices Meet. **32**, 24–27 (1986).
[22]J. Dziewior and D. Silber, Appl. Phys. Lett. **35**, 170–172 (1979).
[23]A. Neugroschel, IEEE Electron Device Lett. **6**, 425–427 (1985).
[24]A. B. Sproul, M. A. Green, and A. W. Stephens, J. Appl. Phys. **72**, 4161–4171 (1992).
[25]D. D. Tang, F. F. Fang, M. Scheuermann, T. C. Chen, and G. Sai-Halasz, Int. Electron Devices Meet. **32**, 20–23 (1986).
[26]J. Wagner and J. A. del Alamo, J. Appl. Phys. **63**, 425–429 (1988).
[27]M. Y. Ghannam and R. P. Mertens, in *22nd European Solid State Device Research Conference, 1992, ESSDERC '92* (IEEE, 1992), pp. 691–694.
[28]J. W. Slotboom and H. C. de Graaff, Solid-State Electron. **19**, 857–862 (1976).
[29]R. R. King and R. M. Swanson, IEEE Trans. Electron Devices **38**, 1399–1409 (1991).
[30]W. P. Dumke, J. Appl. Phys. **54**, 3200–3202 (1983).